Structural Interpretation of *J* Coupling Constants in Guanosine and Deoxyguanosine: Modeling the Effects of Sugar Pucker, Backbone Conformation, and Base Pairing

Zuzana Vokáčová,*,† F. Matthias Bickelhaupt,*,‡ JiYí Šponer,§ and Vladimír Sychrovský*,†

Institute of Organic Chemistry and Biochemistry, v.v.i., Academy of Sciences of the Czech Republic, Flemingovo Square 2, 166 10 Prague 6, Czech Republic, Theoretical Chemistry and Amsterdam Center for Multiscale Modeling, Scheikundig Laboratorium der Vrije Universiteit, De Boelelaan 1083, NL-1081 HV Amsterdam, The Netherlands, and Institute of Biophysics, v.v.i., Academy of Sciences of the Czech Republic, Královopolská 135, 612 65 Brno, Czech Republic

Received: March 19, 2009; Revised Manuscript Received: May 20, 2009

The ^3J(C8−H1′), ^3J(C4−H1′), ^1J(C8−H8), ^1J(C1′−H1′), ^1J(C2′−H2′), and ^1J(C2′−H2′2) indirect scalar coupling constants were calculated with the density functional theory in the deoxyguanosine and riboguanosine molecules. The following geometry descriptors were considered in analysis of the structural dependence of the six *J* couplings: the glycosidic torsion angle χ and conformation of the hydroxymethyl group at the C4′ carbon of sugar mimicking the backbone residue and the sugar pucker (C2′-, C3′-endo). The ^3J(C8−H1′) and ^3J(C4−H1′) couplings, which are typically assigned to the χ torsion, also depended on the sugar pucker, although the calculated dependence of the latter coupling on sugar pucker was nearly negligible. New parametrization of the Karplus equations, taking into account the stereoinversion effect at the glycosidic nitrogen atom and solvent effects, was calculated for the ^3J(C8−H1′) and ^3J(C4−H1′) coupling assigned to the χ torsion. The calculated phase shift of χ torsion angle in these new Karplus equations was larger by ∼10° compared to its commonly accepted value of 60° (Wijmenga, S. S.; van Buuren, B. N. M. *Prog. NMR Spectrosc.* **1998**, *32*, 287.). The calculated ^1J(C2′−H2′) and ^1J(C2′−H2′2) coupling dominantly depended on the sugar type (deoxyribose or ribose) and its pucker, while the ^1J(C1′−H1′) and ^1J(C8−H8) coupling dominantly depended on the glycosidic torsion angle, although quantitatively, all four ^1J couplings depended on both geometry parameters. The dependences of j-couplings on the torsion angle χ calculated in isolated nucleosides were compared with those taking into account the effect of base pairing occurring in the WC/SE RNA base pair family, which appeared to be minor. The calculated ^3J couplings agreed well with available experimental data similarly as the ^1J couplings, although lack of experimental data diminished more reliable validation of the later couplings.

1. Introduction

Biochemical properties and biological functions of the nucleic acids (NAs) are strongly related to their structural dynamics. One of the relevant possibilities of how NAs can be studied in aqueous solution is offered by NMR spectroscopy.[1,2]

The nucleoside unit is a basic building block of NAs. The measurements of *J* couplings in NAs can provide local information about the geometry parameters between coupled nuclei. The three-bond *J* couplings (^3J couplings) are typically used for determining the torsion angles in both NAs and peptides. For example, the ^3J(C8−H1′) and ^3J(C4−H1′) couplings are assigned to the glycosidic torsion angle in nucleosides. However, also, other kinds of *J* couplings can be used for determining the geometry of NA molecules. For example, the ^2J and ^4J couplings, which were recently calculated in structural patterns of rRNA, showed their dependences on magnitudes of the NA backbone torsion angles.[3] Complex analysis of the sugar-to-base orientation in nucleosides with NMR can provide not only important local structural information, but it can also substantially help to refine the global topologies of NAs and to link the structure with its dynamics. Both types of sugar appearing in the deoxyguanosine (dG) and guanosine (rG), the respective DNA and RNA nucleoside, were investigated in this work. Their main geometry parameters (Figure 1) are the glycosidic torsion angle χ and the sugar pucker conformation (Figure 2). It is well established that RNA with ribose prefers the C3′-endo conformation as dominant, while DNA with deoxyribose mostly populates the C2′-endo arrangements. However, in noncanonical regions of functional RNA molecules C2′-endo is a rather frequent minor sugar pucker conformation that is essential for

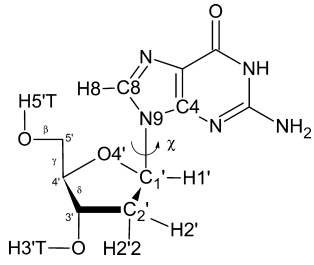

Figure 1. Sketch of the deoxyguanosine molecule with numbering of atoms and torsion angles; χ = O4′−C1′−N9−C4′, χ' = H1′−C1′−N9−C8 + 60°, β = H5′T−O5′−C5′−C4′, γ = O5′−C5′−C4′−C3′, δ = C5′−C4′−C3′−O3′.

* To whom correspondence should be addressed. E-mails: zuzana.vokacova@uochb.cas.cz (Z.V.), FM.Bickelhaupt@few.vu.nl (F.M.B), vladimir.sychrovsky@uochb.cas.cz (V.S.).

† Institute of Organic Chemistry and Biochemistry, v.v.i., Academy of Sciences of the Czech Republic.

‡ Scheikundig Laboratorium der Vrije Universiteit.

§ Institute of Biophysics, v.v.i., Academy of Sciences of the Czech Republic.

10.1021/jp902473v CCC: $40.75
Published on Web 07/01/2009

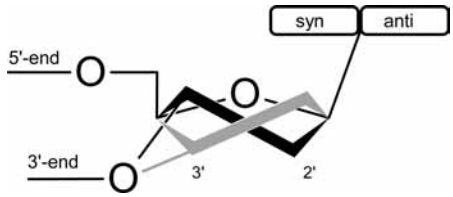

Figure 2. Schematic representation of the C2′-endo (gray) and C3′-endo (black) sugar pucker corresponding to the South and North conformation, respectively, and definition of the syn ($50° < \chi < 80°$) and anti ($180° < \chi < 280°$) regions of χ torsion, describing different orientations of the nitrogenous base with respect to sugar.

important noncanonical segments and RNA building blocks,[4,5] while, for example, A-DNA and A to B intermediate DNA structures are characterized by A-like C3′-endo puckers.[6,7] The effect of the sugar puckering and the sugar-to-base orientation on NMR parameters has been studied extensively both experimentally[8−14] and theoretically.[1,15−19]

A rather basal prerequisite for an accurate structural interpretation of NMR experimental data is to describe correctly all effects which can influence the magnitudes of measured NMR parameters. Obviously, one needs to first know the basic dependence on the assigned geometry parameter. However, this primary dependence can be substantially modulated by other structural parameters due to the natural complex flexibility of nucleic acids.[20,21] Also, proper inclusion of solvent seems to be essential for accurate calculations of the NMR parameters.[17]

In this work, we address the issue of accuracy of the fitted Karplus equations using comprehensive modeling of both the local geometry and solvent effects. The empirical Karplus equations derived with the experimental data commonly suffer from an insufficient number of well-resolved points used for their fitting. The quality of the fit depends crucially on the number of available experimental data points (typically the ^3J coupling/torsion angle). Such benchmark cases unfortunately offer rather limited variation in the structural coordinate since they mostly correspond to molecules with a multiply validated geometry like the Dickerson dodecamer, in order to prevent misinterpretation of the experimental data. Further, a priori known torsion angles which can be used for the fitting do not have to sufficiently characterize all important conformational regions. Typical well-established classes of NAs with well-defined geometries like A-, B-, or Z-DNA and A-RNA with canonical base pairs offer only narrow ranges of χ torsion within the syn or anti region (Figure 2).[18] On the other hand, especially RNA molecules offer astonishing variability of local structures as well as global folding topologies associated with wide ranges of dynamical behavior where sampling of a more complex distribution of the glycosidic torsions can be expected. Theoretical parametrizations of the Karplus curves, which take into account all important geometry parameters in a complex way, thus can improve their accuracy and reliability. Theory can further model the trends in J couplings by solvation or different solute−solvent interactions, providing thus an estimate of robustness for the calculated dependencies of NMR parameters.

A comprehensive computational study of the six J couplings in the dG and rG nucleosides carried out in this study was focused on the following structural features and effects: (i) variation of the glycosidic torsion angle χ, (ii) effect of the B- and Z-DNA backbone conformations considered for the hydroxymethyl group at the C4′ carbon of the sugar moiety, (iii) effect of sugar specificity in the deoxyribose (dG) and ribose (rG) nucleosides, (iv) effect of sugar pucker (C2′-, C3′-endo), (v) effect of solvent (gas-phase versus implicit model of water solvent), and (vi) effect of base pairing in non-Watson−Crick RNA base pairs (Figure 3). The later task is motivated by the fact that folded RNA molecules contain a wide range of functionally important non-Watson−Crick base pairs (altogether, six geometrical families) that directly include the ribose via its 2′-hydroxyl group in base pairing.[22] The noncanonical base pairs are of primary importance in building up key functional RNA building blocks,[23] while their direct identification by NMR techniques is not straightforward.[24]

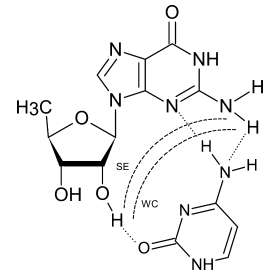

Figure 3. Sketch of the Watson−Crick/sugar edge (WC/SE) cytosine/guanine base pair including putative noncovalent interactions (dotted lines).

2. Methods Section

All geometries were optimized with the B3LYP functional and the 6-31G** basis set. The glycosidic torsion χ was varied stepwise as the main geometry parameter (the χ scans). The other geometry parameters were either kept fixed in each step (backbone, see below) or relaxed (sugar pucker and all remaining geometry parameters), thus giving rise to separate χ scans (Supporting Information).

The hydroxymethyl group at the C4′ carbon of sugar modeling of the part of NA backbone was kept fixed in the geometry corresponding to B-DNA ($\beta = 176°$, $\gamma = 48°$, Figure 1), Z-DNA ($\beta = 183°$, $\gamma = 179°$), and A-RNA ($\beta = 173°$, $\gamma = 54°$). Two separate χ scans with the C2′- or C3′-endo sugar pucker (Figure 2) were carried out for all dG and rG nucleosides. We note that the sugar moiety preserved its starting conformation C2′- or C3′-endo obtained for the global minima structure and did not interconvert when the χ torsion was smoothly varying. The geometries of the B-DNA dG nucleosides were obtained previously[20] as well as the geometries of the WC/SE base pairs.[25,26]

The NMR scalar spin−spin coupling constants[27,28] were computed using the coupled perturbed density functional theory (CP-DFT) method[29,30] with the B3LYP functional, which was found to possess the best overall performance among other commonly used DFT functionals,[29,30] and the IgloIII basis set[31] by including all four J coupling terms (DSO, PSO, FC, SD). The ^nJ(X,Y) couplings in units of Hz were calculated between atoms X and Y (actually the ^{1}H or ^{13}C isotopes) separated by n bonds.

The geometries were optimized in the gas phase, and J coupling were computed both in the gas phase and with the polarized continuum model of water (PCM)[32] added subsequently for the gas-phase equilibrium geometries.

The effect of atomic basis set size on the magnitude of the J couplings was calculated for the B-DNA guanosine with C2′-endo sugar ($\chi = 239.1°$, global energy minimum). The difference between J couplings calculated with the Iglo II and Iglo III bases was smaller than 0.1 and 1.8 Hz for the ^3J and ^1J couplings, respectively. This basis set effect corresponding roughly to the relative error of 1% is in agreement with our previous study.[3]

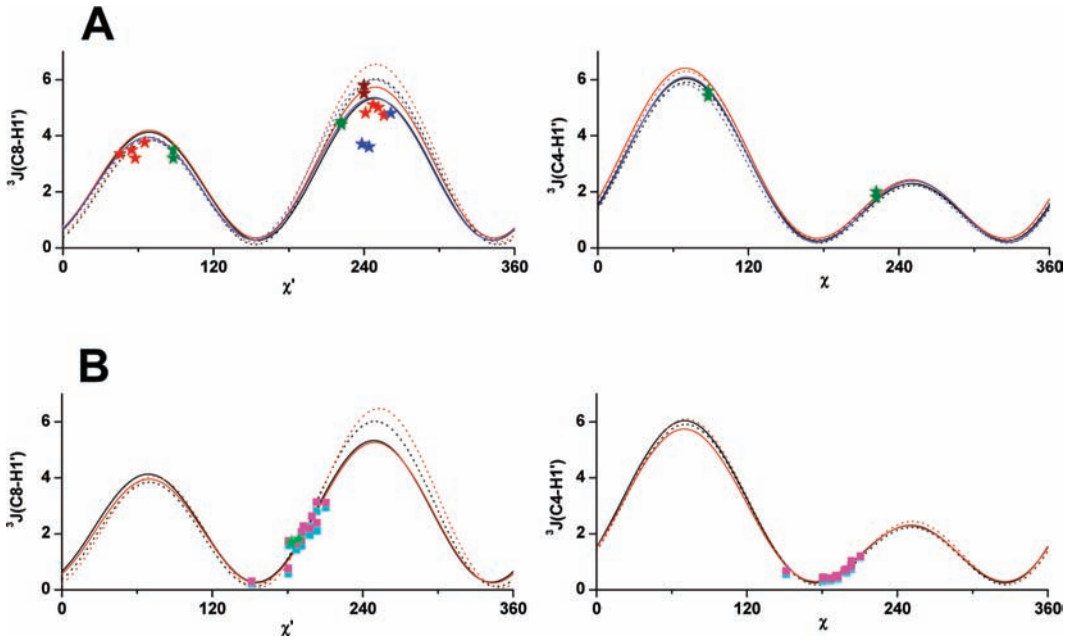

Figure 4. The fitted Karplus equations for the ^3J(C8−H1′) and ^3J(C4−H1′) coupling constants in Hz plotted as function of the χ' (χ' = H1′−C1′−N9−C8 + 60°)[16] and the χ (the glycosidic torsion) angle in degrees, respectively. The C2′- and C3′-endo sugar pucker conformations correspond to the solid and dotted lines, respectively. (A) The dG nucleosides; B-DNA without solvent (black), B-DNA including PCM solvent (red), and Z-DNA without solvent (blue). (B) The rG nucleosides; B-DNA without solvent added for comparison (black), A-RNA without solvent (red), and WC/SE base pairs without and including water solvent (blue and magenta squares, respectively). The experimental ^3J couplings in DNA (red,[18] olive,[34] blue,[14] and brown[35] asterisk) and RNA (green asterisk[12]).

All calculations were done with the Gaussian 03 program package.[33]

All calculated *J* couplings are listed in the Supporting Information (Tables S1−S10).

3. Results and Discussion

The three-bond couplings ^3J(C8−H1′) and ^3J(C4−H1′) across the glycosidic linkage are usually assigned to the χ torsion. In this work, we analyzed the finer effects of the backbone conformation, composition of sugar, and its pucker, base pairing, and solvent on the primary dependence of the six *J* coupling constants on the glycosidic torsion angle χ in the dG and rG nucleosides. The three-bond couplings ^3J(C8−H1′) and ^3J(C4−H1′) across the glycosidic linkage are typically assigned to the χ torsion. Such structural dependence of the one-bond couplings ^1J(C2′−H2′), ^1J(C2′−H2′2), and ^1J(C8−H8) in NA nucleosides was, to our best knowledge, studied in this work for the first time. Dependence of the two ^3J couplings and the ^1J(C1′−H1′) coupling on the χ torsion only was studied previously in the DNA nucleosides.[16] By including also the other ^1J couplings in this study focused on determination of the χ torsion, we would like to expand our knowledge about their dependence on this basic structural descriptor in NA nucleosides.

3.1. The ^3J Couplings. Dependence of the ^3J(C8−H1′) and ^3J(C4−H1′) couplings on the glycosidic torsion is large and actually dominates among the dependencies on other geometry parameters, as has been shown in the earlier studies.[1,15,16] This can be expected since the spin−spin coupling pathway of the two ^3J couplings and atoms defining the χ torsion mostly coincide. Munzarová et al.[16] recently suggested new theoretical Karplus equations for the two ^3J couplings which were specific with regard to the kind of base in the DNA nucleosides.[16] The effect of sugar pucker on the magnitude of the ^3J(C8−H1′) and ^3J(C4−H1′) couplings (smaller than 0.8 Hz) was reported just for two geometries corresponding to the energy minima in the syn and anti region.[16]

Before we proceed to discussion on the calculated ^3J couplings, we comment on their individual assignment to torsion angles. The ^3J(C4−H1′) coupling was assigned to the χ torsion, although the atoms defining χ torsion (O4′−C1′−N9−C4) are not the same as the spin−spin pathway of the ^3J(C4−H1′) coupling (Figure 1). The ^3J(C8−H1′) coupling requires special assignment to the appropriate torsion angle. We used for this purpose the χ' torsion; this torsion equals χ only upon exact nucleobase planarity at nitrogen N9 (Figure 1). The same assignment was actually used previously by Munzarova et al.[16] (See also the section 3.2.)

The calculated dependencies of the two ^3J couplings on the χ- and χ' torsion angles show basically the same shape, but their calculated dependence on the sugar pucker differs (Figure 4). The calculated profile of the ^3J(C4−H1′) coupling was less dependent on the conformation of sugar than the ^3J(C8−H1′) one, in agreement with the calculations by Munzarová.[16] The changes in magnitudes of both ^3J couplings due to different sugar pucker were overall smaller than 0.4 and 0.8 Hz for the ^3J(C4−H1′) and ^3J(C8−H1′) coupling, respectively. Both ^3J couplings calculated within the syn region of χ torsion in the C3′-endo B-DNA nucleosides are smaller compared to the C2′-endo ones, while the opposite trend was calculated in the anti region, again in agreement with Munzarová's study.[16] The sugar pucker effect on both ^3J couplings was negligible when χ torsion was in between the syn and anti regions. The same trend was actually obtained in the Z-DNA dG nucleosides and also when the PCM model of water solvent was applied (Figure 4).

Application of the PCM solvent led to the increase of the two calculated ^3J couplings independent of sugar pucker, which ranged from 0.1 to 0.4 Hz. The calculated trends were the same in both dG and rG nucleosides.

Surprisingly, the base pairing interactions in the direct and water-mediated *cis*-WC/SE G/rG base pairs (selected as a representative example of base pairs interacting via their sugar edges) did not modify the trends calculated for isolated

nucleosides (Figures 4B and 6). The ^3J couplings calculated in the WC/SE base pairs nicely fit the trends shown by the fitted Karplus equations, although the sugar edge is relatively close to the glycoside bond of the rG nucleoside.

Available experimental data[12,14,18,34,35] agree well with the calculated dependencies (Figure 4). Probably the best agreement with experiment was achieved for the ^3J(C8−H1′) and ^3J(C4−H1′) couplings measured in DNA G quartet.[10,34] To our best knowledge, the only experimental value of the ^3J(C8−H1′) couplings measured in RNA by Hines et al.[12] perfectly agrees with the calculated coupling (Figure 4B). The ^3J(C8−H1′) (4.4 ± 0.1 Hz) and ^3J(C4−H1′) (2.8 ± 0.4 Hz) couplings measured in RNA by Schwalbe et al.[36] could not be correlated with molecular structure since the torsion in a mononucleoside shows conformational averaging; nevertheless, the measured ranges basically agree with our calculations.

3.2. Parametrization of Karplus Equations for the ^3J Coulings. The mathematical form of how the ^3J couplings depend on the corresponding torsion angle suggested first by Karplus[37,38]

$$^3J(\mathrm{C}n - \mathrm{H1}') = A\cos^2(\chi - \varphi) + B\cos(\chi - \varphi) + C \quad (1)$$

was also adopted here for the ^3J(Cn−H1′), n = 4, 8, couplings. The amplitudes A and B and parameter C are normally fitted on the basis of measurements (the empirical Karplus equation), while the phase shift φ is usually considered constant. Alternatively, they can be fitted for the calculated data points. The magnitude of the φ shift corresponds here to the difference between the χ torsion and the actual torsion angle probed with J coupling, which is given by the three bonds interconnecting the Cn−H1′, n = 4, 8, atoms. In this case, the χ torsion (O4′−C1′−N9−C4) differs from the spin−spin pathway of the ^3J(C4−H1′) and ^3J(C8−H1′) couplings by about 60 and 120°, respectively.

The accuracy of the torsion angles resolved in practice with measured ^3J couplings depends on the quality of the fitted Karplus curve. The validity and robustness of the fit with respect to complex geometry parameters or solute−solvent interactions is therefore worthwhile to model since such effects may lower the quality of the outgoing NMR structural data.

As was mentioned, the φ phase shift in empirical Karplus equations is usually fixed to a certain value, which can be expected from the steric arrangement of atoms and corresponds to the difference between the assigned and "NMR probed" torsion angle (Ipel,[9,10] Wijmenga,[1] Trantírek;[18] eqs 2−5). However, Munzarová et al.[16] pointed out that the φ phase shift of the ^3J(C4−H1′) coupling assigned to the χ torsion actually deviates from the ideal magnitude of 60° when included in the fitting procedure (eqs 6 and 7).

$$^3J_{\mathrm{Wijmenga}}(\mathrm{C4} - H1') = 4.7\cos^2(\chi - 60°) + 2.3\cos(\chi - 60°) + 0.1 \quad (2)$$

$$^3J_{\mathrm{Wijmenga}}(\mathrm{C8} - H1') = 4.5\cos^2(\chi - 60°) - 0.6\cos(\chi - 60°) + 0.1 \quad (3)$$

$$^3J_{\mathrm{Trantirek}}(\mathrm{C4} - H1') = 4.4\cos^2(\chi - 60°) + 1.4\cos(\chi - 60°) + 0.1 \quad (4)$$

$$^3J_{\mathrm{Trantirek}}(\mathrm{C8} - H1') = 4.1\cos^2(\chi - 60°) - 0.7\cos(\chi - 60°) + 0.1 \quad (5)$$

$$^3J_{\mathrm{Munzarova}}(\mathrm{C4} - H1') = 3.6\cos^2(\chi - 68.6°) + 1.8\cos(\chi - 68.6°) + 0.4 \quad (6)$$

$$^3J_{\mathrm{Munzarova}}(\mathrm{C8} - H1') = 4.2\cos^2(\chi' - 68.9°) - 0.5\cos(\chi' - 68.9°) + 0.3 \quad (7)$$

We note that the φ phase shift of +60° (+68.9° in eq 7) used consistently in Karplus curves for both the ^3J(C4−H1′) and ^3J(C8−H1′) couplings (as was suggested first by Ippel[10] and Wijmenga[1]) instead of the −120° shift for the later J coupling corresponds to the negative sign of the B coefficient (eqs 3, 5, and 7). The amplitudes and phase shifts (Tables 1 and 2) were fitted for the calculated data (Supporting Information) with the Levenberg−Marquardt procedure combined with the simplex iteration method using the Microcal(TM) Origin 6.0 program. The interval calculated for the χ torsion (0−360°) was expanded symmetrically by one 360° period before and after this interval prior to the fitting. The overall quality of the fitted parameters shown in Tables 1 and 2 was very good (R^2 = 0.9881−0.9980, χ^2 = 0.0330−0.0073). We note that the ^3J(C4−H1′) coupling was assigned to the χ torsion, while the ^3J(C8−H1′) coupling was fitted as dependent on the χ' torsion. The χ and χ' torsion angles are far from being the same for different sugar-to-base orientations, and therefore, the ^3J(C8−H1′) coupling has to be assigned to the χ' torsion, which directly corresponds to the spin−spin coupling pathway (Figures 1 and 4).

TABLE 1: The Parameters A, B, and C in Hz and the Phase φ in Degrees of Karplus Equations for the ^3J(C4−H1′) Coupling Assigned to the O4′−C1′−N9−C4 Dihedral Angle (the glycosidic torsion χ)

nucleoside	sugar conformation	solvent	A	B	C	φ
B-DNA	C2′-endo		3.68	1.87	0.49	70.44
B-DNA	C3′-endo		3.66	1.84	0.41	71.11
B-DNA	C2′-endo	water	3.82	1.99	0.60	69.71
B-DNA	C3′-endo	water	3.82	1.95	0.53	70.56
Z-DNA	C2′-endo		3.82	1.85	0.42	70.62
Z-DNA	C3′-endo		3.61	1.78	0.45	68.26
A-RNA	C2′-endo		3.50	1.73	0.51	70.09
A-RNA	C3′-endo		3.86	1.83	0.41	71.68
B-DNA[a]	C2′-endo		3.6	1.8	0.4	68.9

[a] Reference 16.

TABLE 2: The parameters A, B, and C in Hz and the Phase φ in Degrees of Karplus Equations for the ^3J(C8−H1′) Coupling Assigned to the H1′−C1′−N9−C8 + 60° Dihedral Angle

nucleoside	sugar conformation	solvent	A	B	C	φ
B-DNA	C2′-endo		4.44	−0.60	0.29	68.89
B-DNA	C3′-endo		4.75	−1.09	0.18	69.90
B-DNA	C2′-endo	water	4.57	−0.77	0.39	68.92
B-DNA	C3′-endo	water	4.96	−1.30	0.29	69.31
Z-DNA	C2′-endo		4.34	−0.71	0.31	67.58
Z-DNA	C3′-endo		4.57	−1.07	0.37	67.40
A-RNA	C2′-endo		4.34	−0.66	0.27	69.71
A-RNA	C3′-endo		5.12	−1.22	0.14	73.06
B-DNA[a]			4.2	−0.5	0.3	68.9

[a] Reference 16.

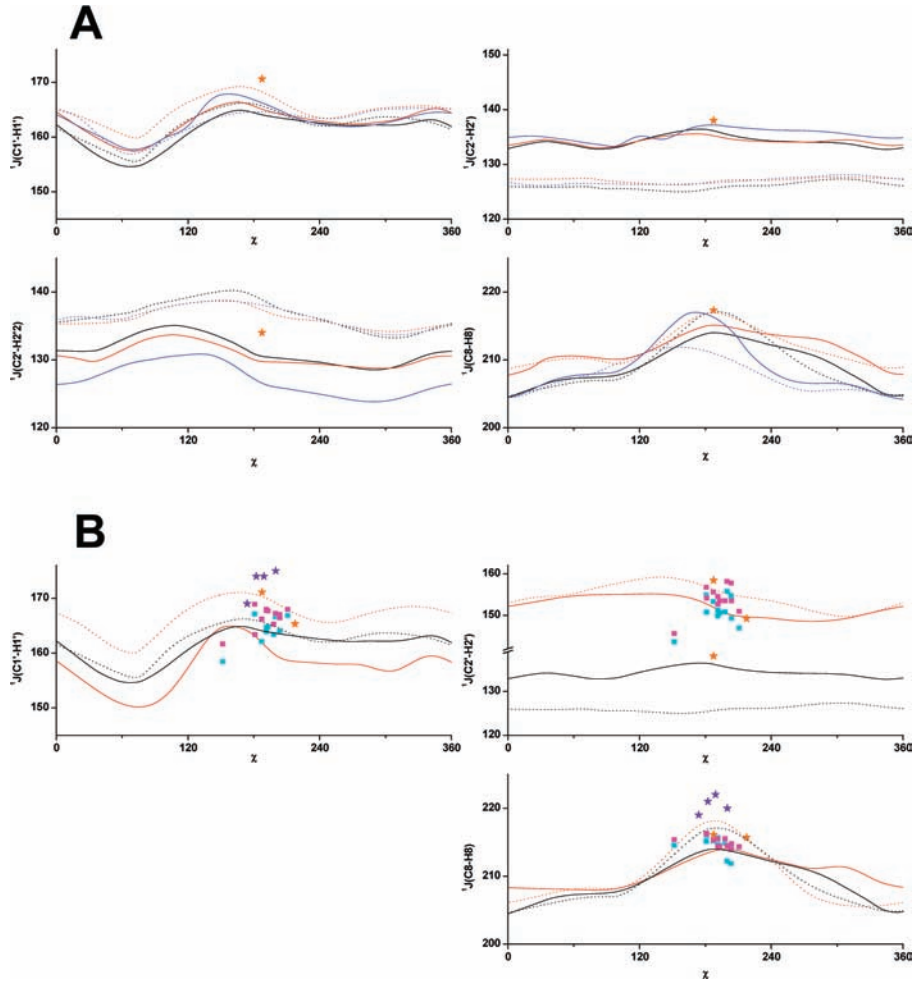

Figure 5. The calculated dependence for the ^1J(C1′−H1′), ^1J(C2′−H2′), ^1J(C1′−H2′2), and ^1J(C8−H8) coupling constants in Hz plotted as function of the χ (the glycosidic torsion) angle in degrees. The C2′- and C3′-endo sugar pucker conformations correspond to the solid and dotted lines, respectively. (A) The dG nucleosides; B-DNA without solvent (black), B-DNA including PCM solvent (red), and Z-DNA without solvent (blue). (B) The rG nucleosides; B-DNA without solvent added for comparison (black), A-RNA without solvent (red), and WC/SE base pairs without and including water solvent (blue and magenta squares, respectively). The experimental ^3J couplings in DNA (orange asterisk[10]) and RNA (orange[10] and violet[42] asterisk).

Different sugar pucker of the dG and rG nucleosides had an effect on the fitted amplitudes in the Karplus equations for the ^3J(C8−H1′) coupling. The absolute amplitudes *A* and *B* fitted in the C2′-endo nucleosides were consistently smaller compared to those calculated for the C3′-endo nucleosides (Table 1). The amplitudes obtained for the ^3J(C4−H1′) coupling were more independent of sugar pucker, except for the dG nucleoside with the Z-DNA backbone (Table 2). The Karplus equations fitted here for the two sugar puckers reflect the trend calculated by Munzarová.[16]

Application of the implicit water solvent led to the increase of the ^3J(C4−H1′) and ^3J(C8−H1′) couplings relative to the gas-phase values by as much as 0.16 and 1 Hz, respectively. This increase was reflected by the increase of absolute magnitudes of the *A* and *B* amplitudes (Tables 1 and 2).

The fitted φ phase shift ranged from 67.4 to 73.1°, which is in agreement with the values calculated by Munzarová[16] (Tables 1 and 2). Also, the fitted amplitudes for the two ^3J couplings are close to those which were obtained by Munzarová.[16] This together indicated that (a) the φ phase shift should be included as a "free" parameter into the fitting procedure for the $^3J/\chi$ Karplus equations and (b) the obtained Karplus equations are sufficiently robust with respect to the geometry and solvent effects modeled in this work.

3.3. The ^1J Couplings. The ^1J(C1′−H1′) and ^1J(C8−H8) couplings should depend dominantly on the glycosidic torsion, while the ^1J(C2′−H2′) and ^1J(C2′−H2′2) ones should depend dominantly on the sugar pucker.[1,10,39]

The **^1J(C1′−H1′)** couplings calculated in the dG and rG nucleosides ranged from 154 to 170 Hz. The smaller magnitudes were calculated in the *syn*-nucleosides, while the maximal magnitudes of the *J* coupling were calculated near the anti region for $\chi \approx 180°$ (Figure 5). The magnitudes of the ^1J(C1′−H1′) coupling measured in the *anti*-guanosines by Kline[8] or Varani and Tinoco[40] and also in other nucleosides[8,10,39,41] were similar to the calculated range. Specificity of the NA base should not therefore significantly affect the ^1J(C1′−H1′) coupling magnitude.

Application of the implicit water solvent led to the increase of the calculated ^1J(C1′−H1′) coupling by as much as 4.4 Hz in the syn region (Figure 5). In the anti region, near $\chi \approx 240°$, the effect of implicit solvent was damped down. This happened probably due to the close spatial proximity of the H1′ and N3 atoms, which may hinder effective polarization of the C1′−H1' bond by the implicit solvent cavity. Magnitudes of the ^1J(C1′−H1′) couplings calculated in the C3′-endo nucleosides were overall larger roughly by 2 Hz in comparison with those calculated in the C2′-endo nucleosides. The larger effect of sugar pucker was calculated in the syn region of the rG nucleosides

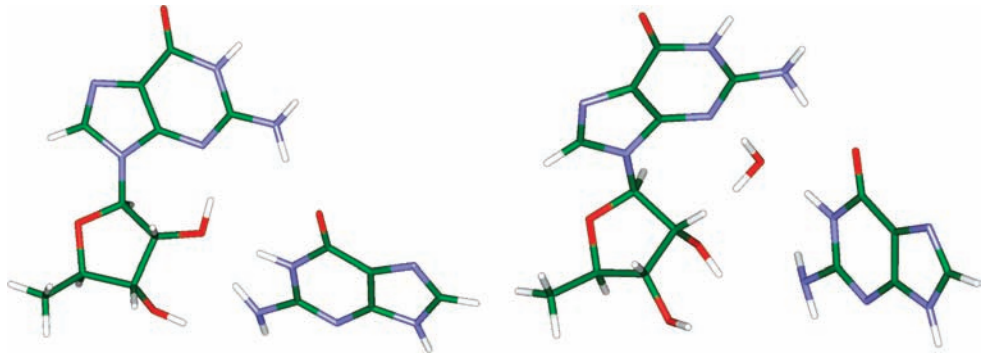

Figure 6. Molecular complexes of the *cis*-Watson−Crick/sugar edge G/rG base and its water-mediated substate (right).[25]

compared to the dG ones (Figure 4A, B). The ^1J(C1′−H1′) couplings calculated in the rG nucleoside were smaller at most by 5 Hz than those calculated in the dG one, except for the region with $\chi \approx 180°$ where the magnitudes calculated in both nucleosides were almost the same (Figure 5B).

Except for the parametrization by Munzarová[16] for the ^1J(C1′−H1′) coupling,[16] no other parametrizations for the Karplus equations for any of the four ^1J couplings were reported. Although the overall trend calculated for the ^1J(C1′−H1′) coupling is very similar to the trend obtained by Munzarová, the magnitudes calculated by Munzarová are systematically smaller approximately by 10 Hz. Since our calculations of the ^1J(C1′−H1′) coupling correspond well with the experiment,[10,36,42] the underestimated trend calculated previously by Munzarová was most probably caused by some systematic error which is difficult for us to clarify since they used a different calculation method and software.

The calculated **^1J(C8−H8)** couplings ranged from 204 to 218 Hz, which is in qualitative agreement with a few experiments available for this ^1J couplings in the literature reporting the range from 215.7 to 222 Hz.[10,11] The calculated dependence on the χ torsion had one maximum near 180° and one minimum near 0/360° (Figure 5). The two extremes of the calculated dependence actually correspond to the planar arrangement of the H8−C8−N9−C1′−O4′ covalently linked atoms. The C2′/C3′-endo sugar pucker effect on the calculated ^1J(C8−H8) couplings was opposite in the decaying part of the dependence and near the maximum where the curves calculated in the C3′-endo nucleosides actually dominated (at most by 3 Hz) over those calculated in the C2′-endo ones (Figure 5A). The ^1J(C8−H8) couplings calculated for the $\chi \approx 0°$ in the rG nucleoside were smaller than those in the dG nucleoside, but near $\chi \approx 180°$, both calculated dependencies almost coincided (Figure 5B). The ^1J(C8−H8) coupling measured in the dG and rG nucleoside of the same molecule, the circular r< pGp(dG)> dinucleoside, was 216.1 and 217.3 Hz, respectively.[10] Both nucleosides in the r<pGp(dG)> molecule had the same torsion angle of $\chi = 187.5°$ (SIWWOK in the Cambridge Database[43,44]). Practically the same magnitudes of the ^1J(C8−H8) coupling measured in the r<pGp(dG)> molecule with a well-resolved value of the χ torsion correlate nicely with our calculations.

Other values of the ^1J(C8−H8) coupling measured in guanosines were 215.7 Hz in cyclic trinucleoside,[10] 216.0 Hz in guanosine monophosphate,[10] and 214.85 Hz in the RNA oligomer from the helix-35 of *E. coli* 23S rRNA.[11]

The ^1J(C8−H8) couplings calculated with the inclusion of implicit water solvent were overall larger than those obtained in the gas-phase calculations (at most by 4 Hz) and ranged from 207 to 218 Hz. This is in agreement with our previous study of the ^1J(C8−H8) coupling in the DNA hairpin molecule.[17] Modifications of the β and γ torsion angles (Figure 1) in the dG nucleosides, which reflects their orientation in the B- or Z-DNA backbone, had inconsiderable impact on the curvature of the calculated dependences (Figure 5A).

The calculated **^1J(C2′−H2′)** and **^1J(C2′−H2′2)** couplings strongly depended on the sugar type and conformation (Figure 5).

The ^1J(C2′−H2′) couplings calculated in the dG nucleoside (the gas-phase calculation) ranged from 132.4 to 137.2 Hz and from 124.7 to 128.5 Hz for the C2′- and C3′-endo sugar puckers, respectively. Similar separation of the dependencies with different sugar pucker was calculated also for the ^1J(C2′−H2′2) couplings ranging from 123.7 to 135.2 Hz (C2′-endo), and from 133.0 to 140.7 Hz (C3′-endo). The calculated trends agreed with the ^1J(C2′−H2) and ^1J(C2′−H2′2) couplings measured by Ippel.[10] The effect of the implicit solvent on the calculated magnitudes of both ^1J couplings was negligible in comparison with the effects of sugar pucker and backbone torsion variation.

A different kind of sugar in the dG and rG nucleosides had a large impact on the calculated ^1J(C2′−H2) and ^1J(C2′−H2′2) couplings (Figure 5B). For the ^1J(C2′−H2′) coupling in the dG and rG nucleoside, the calculated mean values differed by 20 and 29 Hz for the C2′- and C3′-endo sugar puckers, respectively. This trend calculated for the ^1J(C2′−H2′) coupling agrees with the 138 ± 2 and 158.4 ± 0.5 Hz couplings measured in the r<pGp(dG)> molecule for the dG and rG nucleoside,[10] respectively. The ^1J(C2′−H2′) coupling of 138 Hz and the ^1J(C2′-H2′2) one of 134 Hz, which were measured in the r<pGp(dG)> molecule, would therefore, according to our calculations, indicate the C2′-endo sugar pucker of the dG nucleoside rather than C3′-endo one (Figure 5).

3.4. Impact of Base Pairing and Explicit Water Molecules on the Magnitude of the *J* Constants. Base pairing belongs to the essential interactions which stabilize the structure of the polynucleotides in DNA and RNA molecules. Modeling the effect of various base pairing interactions on *J* coupling magnitudes would therefore confront the trends obtained in bare nucleosides with those in realistic structural patterns occurring in NAs.

As a structural models for such a theoretical NMR study, we adopted the RNA Watson−Crick/sugar edge (WC/SE)[22] class of base pairs (Figures 3 and 6), which was also intensively studied previously.[26,45] We selected actually the 12 WC/SE base pairs in which the rG nucleoside interacts via its SE with all other nucleobases. This class of extended RNA base pairing interactions is highly relevant for the purpose since (a) the noncovalent interactions in the WC/SE base pairs occur in the proximity of the glycosidic bond, in contrast to the canonical WC/WC interactions, and (b) WC/SE base pairs (and other types of SE base pairs) are common in ribosome and other functional RNAs, as evidenced by the numerous X-ray studies. They are,

in fact, essential for the formation of many functional RNA building blocks and motifs. Thus, characterizing their NMR signatures by calculations can provide an important link between theory and experiment, which can improve the NMR structural analysis of RNAs.

Variation of the glycosidic torsion angle in the WC/SE base pairs (from 150 to 210°) covers the low anti region. The calculated variation of the ^3J(C8−H1′), ^3J(C4−H1′), ^1J(C1′−H1′), ^1J(C2′−H2′), and ^1J(C8−H8) couplings in the WC/SE base pairs was 0.2−3.1, 0.3−1.2, 158.5−169.0, 143.7−158.2, and 211.9−216.3 Hz, respectively. When the WC/SE base pairs were embedded into the implicit water solvent, the absolute magnitudes of the coupling increased very little (Figures 4B and 5B).

The ^3J(C4−H1′) couplings calculated in the WC/SE base pairs fit perfectly the Karplus curves (Figure 4B). The ^3J(C8−H1′) couplings in the WC/SE base pairs probably had more disperse character, but they still fit the Karplus curve very well. Interestingly, the carbon C8 seemed to be more perturbed by the WC/SE base pair interactions than the C4 one, although its spatial proximity to the "perturbing" base in a pair was larger.

The trends calculated for the three ^1J coupings in the rG nucleoside and in the WC/SE base pairs were not qualitatively equivalent. The large impact of the base pairing was calculated especially for the ^1J(C1′−H1′) and ^1J(C2′−H2′) couplings, where the atoms coupled in the spin−spin interaction and the sugar atoms exposed to the sugar edge of the WC/SE base pairs were actually the same (Figures 4B and 5B). If any structural information concerning the glycosidic torsion in the rG nucleosides can be acquired from the three ^1J couplings, it could be easily lost due to the large effect and individual character of the noncovalent interactions in the sugar edge.

Some WC/SE base pairs (and other base pairs involving the sugar edges) had water-mediated contacts between the ribose and base (Figure 6). The balance between direct and water-mediated substates of the base pairs may be important for RNA structural dynamics.[46] The effect of such an explicit water molecule on the *J* couplings can be estimated from the calculations in the *cis*-G/rG base pair (Figure 6). The glycosidic torsion calculated in the *cis*-G/rG complex without and with water molecule was 151 and 181°, respectively. The calculated absolute shift of *J* couplings due to the explicit water in the *cis*-G·rG complex was smaller than 0.6 Hz in the case of the two ^3J coulings and the ^1J(C8−H8) coupling, while for the ^1J(C1′−H1′) and ^1J(C2′−H2′) couplings, it was 8.7 and 11.2 Hz, respectively. The trends calculated for the ^1J(C1′−H1′) and ^1J(C2′−H2′) couplings may therefore require specific calibration, which would be dependent on the topology and mobility of the water solvent molecules that can penetrate into the NA base pairs.

4. Conclusion

We have carried out a comprehensive computational study of the dependence of the ^3J(C8−H1′), ^3J(C4−H1′), ^1J(C1′−H1′), ^1J(C8−H8), ^1J(C2′−H2′), and ^1J(C2′−H2′2) NMR spin−spin coupling constants on the geometry in the dG (deoxyguanosine) and rG (riboguanosine) molecules.

Calculations of the six *J* couplings were focused on their dependence on the following geometry parameters: the glycosidic torsion angle χ, the sugar pucker C2′- and C3′-endo, the β and γ torsion angles of the hydroxymethyl group at the C4′ carbon of sugar used for modeling the effect of different NA backbone geometry (B- and Z-DNA), and the type of sugar (dG, rG). The effect of the base pairing on *J* couplings was calculated for the rG nucleosides in the WC/SE RNA base pairs.

The ^3J(C8−H1′) and ^3J(C4−H1′) couplings depended dominantly on the χ torsion. Sugar pucker of both the dG and rG nucleosides had systematic impact on the calculated χ dependencies of the ^3J(C8−H1′) coupling (the larger magnitudes were obtained in the C3′-endo nucleosides), while the dependence of ^3J(C4−H1′) coupling on sugar pucker was practically negligible (cf. also Munzarová et al.[16]). New Karplus equations respecting sugar pucker in the dG and rG nucleosides taking into account the effect of water solvent were fitted for the two ^3J couplings. The calculated impact of the backbone geometry on the two ^3J couplings was practically negligible, as well as the effect of base pairing in the WC/SE RNA base pairs. This fact better validates use of these Karplus equations in NMR structural studies.

The calculated ^1J(C2′−H2′) and ^1J(C2′−H2′2) couplings depended dominantly on the type of sugar in the rG and dG nucleosides and also on its sugar pucker. The ^1J(C1′−H1′) and ^1J(C8−H8) couplings were more dependent on the glycosidic torsion angle, and qualitatively different dependencies were calculated for the dG and rG nucleosides. The structural information concerning the χ torsion acquired from the three ^1J couplings can be strongly affected by the specificity of the noncovalent interactions in the sugar edge of the rG nucleosides. Calculated dependences of the ^1J couplings thus brought only additional information regarding the possible determination of the glycosidic torsion, which can be nevertheless used as support in the context of better-suited ^3J(C4/C8−H1′) couplings. The three ^1J couplings, however, still represent another, although less significant, NMR structural constraint for the NMR structural studies focused on the glycosidic torsion. For example, the ^1J(C8−H8) coupling changes roughly by 10 Hz when the guanine base adopts orientation with respect to sugar, corresponding to $\chi = 0$ and 180°. The dependences calculated for the six *J* couplings on the χ torsion are in good overall agreement with available experimental data found in the literature.

Acknowledgment. This work was supported by the Academy of Sciences of the Czech Republic (Grant IAA400550701), by the Grant Agency of Charles University (Grant GAUK nr. 58708), by The Netherlands Organization for Scientific Research (NWO-CW), and by the National Research School Combination - Catalysis (NRSC-C). V.S. was supported by a Human Frontier Science Program (HFSP) Young Investigator's Grant. J.S. was also supported by the Academy of Sciences of the Czech Republic, Grants AV0Z50040507 and AV0Z50040702.

Supporting Information Available: All calculated *J* couplings and corresponding geometry parameters. This material is available free of charge via the Internet at http://pubs.acs.org.

References and Notes

(1) Wijmenga, S. S.; van Buuren, B. N. M. *Prog. NMR Spectrosc.* **1998**, *32*, 287.

(2) Alkorta, I.; Elguero, J. *Int. J. Mol. Sci.* **2003**, *4*, 64.

(3) Sychrovský, V.; Vokáčová, Z.; Šponer, J.; Špačková, N.; Schneider, B. *J. Phys. Chem. B* **2006**, *110*, 22894.

(4) Correll, C. C.; Wool, I. G.; Munishkin, A. *J. Mol. Biol.* **1999**, *292*, 275.

(5) Ban, N.; Nissen, P.; Hansen, J.; Moore, P. B.; Steitz, T. A. *Science* **2000**, *289*, 905.

(6) Wahl, M. C.; Sundaralingam, M. *Biopolymers* **1997**, *44*, 45.

(7) Ng, H. L.; Dickerson, R. E. *Nucleic Acids Res.* **2002**, *30*, 4061.

(8) Kline, P. C.; Serianni, A. S. *J. Am. Chem. Soc.* **1990**, *112*, 7373.

(9) Davies, D. B.; Rajani, P.; Maccoss, M.; Danyluk, S. S. *Magn. Reson. Chem.* **1985**, *23*, 72.

(10) Ippel, J. H.; Wijmenga, S. S.; de Jong, R.; Heus, H. A.; Hilbers, C. W.; de Vroom, E.; van der Marel, G. A.; van Boom, J. H. *Magn. Reson. Chem.* **1996**, *34*, S156.
(11) Boisbouvier, J.; Bryce, D. L.; O'Neil-Cabello, E.; Nikonowicz, E. P.; Bax, A. *J. Biomol. NMR* **2004**, *30*, 287.
(12) Hines, J. V.; Landry, S. M.; Varani, G.; Tinoco, I. *J. Am. Chem. Soc.* **1994**, *116*, 5823.
(13) Marino, J. P.; Schwalbe, H.; Griesinger, C. *Acc. Chem. Res.* **1999**, *32*, 614.
(14) Zimmer, D. P.; Marino, J. P.; Griesinger, C. *Magn. Reson. Chem.* **1996**, *34*, S177.
(15) Munzarová, M. L.; Sklenář, V. *J. Am. Chem. Soc.* **2002**, *124*, 10666.
(16) Munzarová, M. L.; Sklenář, V. *J. Am. Chem. Soc.* **2003**, *125*, 3649.
(17) Sychrovský, V.; Schneider, B.; Hobza, P.; Žídek, L.; Sklenář, V. *Phys. Chem. Chem. Phys.* **2003**, *5*, 734.
(18) Trantírek, L.; Štefl, R.; Masse, J. E.; Feigon, J.; Sklenář, V. *J. Biomol. NMR* **2002**, *23*, 1.
(19) Foloppe, N.; Nilsson, L.; MacKerrelJr, A. D., Jr. *Biopolymers* **2002**, *61*, 61.
(20) Sychrovský, V.; Muller, N.; Schneider, B.; Smrecki, V.; Špirko, V.; Šponer, J.; Trantírek, L. *J. Am. Chem. Soc.* **2005**, *127*, 14663.
(21) Bouř, P.; Buděšínský, M.; Špirko, V.; Kapitán, J.; Šebestík, J.; Sychrovský, V. *J. Am. Chem. Soc.* **2005**, *127*, 17079.
(22) Leontis, N. B.; Stombaugh, J.; Westhof, E. *Nucleic Acids Res.* **2002**, *30*, 3497.
(23) Leontis, N. B.; Westhof, E. *Curr. Opin. Struct. Biol.* **2003**, *13*, 300.
(24) Yallurupalli, P.; Moore, P. B. *J. Mol. Biol.* **2003**, *325*, 843.
(25) Šponer, J. E.; Špačková, N.; Kulhánek, P.; Leszczynski, J.; Šponer, J. *J. Phys. Chem. A* **2005**, *109*, 2292.
(26) Šponer, J. E.; Špačková, N.; Leszczynski, J.; Šponer, J. *J. Phys. Chem. B* **2005**, *109*, 11399.
(27) Kaupp, M.; Buhl, M.; Malkin, V. *Calculation of NMR and EPR Parameters—Theory and Applications*; Wiley-VCH Verlag: Weinheim, Germany, 2004.
(28) Helgaker, T.; Jaszunski, M.; Ruud, K. *Chem. Rev.* **1999**, *99*, 293.
(29) Sychrovský, V.; Grafenstein, J.; Cremer, D. *J. Chem. Phys.* **2000**, *113*, 3530.
(30) Helgaker, T.; Watson, M.; Handy, N. C. *J. Chem. Phys.* **2000**, *113*, 9402.
(31) Kutzelnigg, W.; Fleischer, U.; Schindler, M. *NMR - Basis Principles and Progress*; Springer: Heidelberg, Germany, 1990.
(32) Cammi, R.; Mennucci, B.; Tomasi, J. *J. Phys. Chem. A* **2000**, *104*, 5631.
(33) Frisch, M. J.; Trucks, G. W.; Schlegel, H. B.; Scuseria, G. E.; Robb, M. A.; Cheeseman, J. R.; Montgomery, J. A., Jr.; Vreven, T.; Kudin, K. N.; Burant, J. C.; Millam, J. M.; Iyengar, S. S.; Tomasi, J.; Barone, V.; Mennucci, B.; Cossi, M.; Scalmani, G.; Rega, N.; Petersson, G. A.; Nakatsuji, H.; Hada, M.; Ehara, M.; Toyota, K.; Fukuda, R.; Hasegawa, J.; Ishida, M.; Nakajima, T.; Honda, Y.; Kitao, O.; Nakai, H.; Klene, M.; Li, X.; Knox, J. E.; Hratchian, H. P.; Cross, J. B.; Bakken, V.; Adamo, C.; Jaramillo, J.; Gomperts, R.; Stratmann, R. E.; Yazyev, O.; Austin, A. J.; Cammi, R.; Pomelli, C.; Ochterski, J. W.; Ayala, P. Y.; Morokuma, K.; Voth, G. A.; Salvador, P.; Dannenberg, J. J.; Zakrzewski, V. G.; Dapprich, S.; Daniels, A. D.; Strain, M. C.; Farkas, O.; Malick, D. K.; Rabuck, A. D.; Raghavachari, K.; Foresman, J. B.; Ortiz, J. V.; Cui, Q.; Baboul, A. G.; Clifford, S.; Cioslowski, J.; Stefanov, B. B.; Liu, G.; Liashenko, A.; Piskorz, P.; Komaromi, I.; Martin, R. L.; Fox, D. J.; Keith, T.; Al-Laham, M. A.; Peng, C. Y.; Nanayakkara, A.; Challacombe, M.; Gill, P. M. W.; Johnson, B.; Chen, W.; Wong, M. W.; Gonzalez, C.; Pople, J. A. *Gaussian 03*, revision C.02; Gaussian, Inc.: Wallingford, CT, 2004.
(34) Zhu, G.; Live, D.; Bax, A. *J. Am. Chem. Soc.* **1994**, *116*, 8370.
(35) Schmieder, P.; Ippel, J. H.; Vandenelst, H.; Vandermarel, G. A.; Vanboom, J. H.; Altona, C.; Kessler, H. *Nucleic Acid Res.* **1992**, *20*, 4747.
(36) Schwalbe, H.; Marino, J. P.; King, G. C.; Wechselberger, R.; Bermel, W.; Griesinger, C. *J. Biomol. NMR* **1994**, *4*, 631.
(37) Karplus, M. *J. Chem. Phys.* **1959**, *30*, 11.
(38) Karplus, M. *J. Am. Chem. Soc.* **1963**, *85*, 2870.
(39) Davies, D. B.; Maccoss, M.; Danyluk, S. S. *J. Chem. Soc., Chem. Commun.* **1984**, 536.
(40) Varani, G.; Cheong, C. J.; Tinoco, I. *Biochemistry* **1991**, *30*, 3280.
(41) Bandyopadhyay, T.; Wu, J.; Stripe, W. A.; Carmichael, I.; Serianni, A. S. *J. Am. Chem. Soc.* **1997**, *119*, 1737.
(42) Varani, G.; Tinoco, I. *J. Am. Chem. Soc.* **1991**, *113*, 9349.
(43) Allen, F. H.; Bellard, S.; Brice, M. D.; Cartright, B. A.; Doubleday, A.; Higgs, H.; Hummelink, T.; Hummelink-Peters, B. G.; Kennard, O.; Motherwell, W. D. S.; Rodgers, J. R.; Watson, D. G. *Acta Crystallogr.* **1979**, *B35*, 2331.
(44) Allen, F. H.; Davies, J. E.; Galloy, J. J.; Johnson, O.; Kennard, O.; Macrae, C. F.; Mitchell, E. M.; Mitchell, G. F.; Smith, J. M.; Watson, D. G. *J. Chem. Inf. Comput. Sci.* **1991**, *31*, 187.
(45) Vokáčová, Z.; Šponer, J.; Šponer, J. E.; Sychrovský, V. *J. Phys. Chem. B* **2007**, *111*, 10813.
(46) Rázga, F.; Koča, J.; Šponer, J.; Leontis, N. B. *Biophys. J.* **2005**, *88*, 3466.

JP902473V